Electronic structure of MS (M=Ca,Mg,Fe,Mn): X-ray absorption analysis

A. N. Kravtsova, I. E. Stekhin, and A. V. Soldatov*
Faculty of Physics, Rostov State University, 5 Sorge str., Rostov-on-Don 344090, Russia

X. Liu and M. E. Fleet
Department of Earth Sciences, University of Western Ontario, London, Ontario, Canada N6A 5B7
(Received 6 March 2003; revised manuscript received 3 February 2004; published 19 April 2004)

Experimental x-ray absorption spectra were measured near the sulfur K and $L_{2,3}$ edges of MgS, CaS, MnS, and FeS. An agreement between full multiple scattering theoretical simulations and experiment is reached for comparatively large clusters (consisting of 9–13 shells) of sulfides with the NaCl-type structure (MgS,CaS,MnS), while a small cluster of four shells appears sufficient for the NiAs-type structure of FeS. It was shown that in the $Mg_{1-x}Fe_xS$ solid solution, iron sulfide changes its structure from NiAs-type ($B8$) to NaCl-type ($B1$) under the influence of the MgS matrix. The partial electronic densities of unoccupied states have been calculated for MgS and CaS. It is found that the bottom of the conduction band of MgS is formed by Mg s and S s states and of CaS by Ca d states and S d, s, and p states. A special kind of hybridization has been found: it is shown that the sulfur p states are ''squeezed out'' of the energy region of the iron d states.

DOI: 10.1103/PhysRevB.69.134109 PACS number(s): 61.10.Ht, 61.66.Fn

I. INTRODUCTION

The monosulfides of Ca, Mg, and Mn have the rocksalt ($B1$) structure and occur in EH enstatite chondrite meteorites, where they appear to result from metamorphism under very reduced conditions.[1] Manganese sulfide also occurs in low-temperature deposits in the Earth's crust. Iron monosulfide has a hexagonal NiAs-type ($B8$) structure under ambient pressure and temperature. FeS is a nearly ubiquitous phase in most meteorites and is the iron sulfide of lunar rocks. It occurs also, albeit sparingly, in magmatic sulfide assemblages of mafic/ultramafic rocks.

One of the most fruitful methods allowing study of the local arrangement of atoms and electronic structure of the presently investigated compounds is x-ray absorption near-edge structure (XANES) spectroscopy.[2] But, in order to extract the necessary information from the experimental spectra, one needs to perform theoretical analyses. There have been several XANES studies on metal sulfides. In particular, FeS has been investigated by a large number of researchers due to its wide range of interesting properties. Sugiura and co-workers[3–5] were the first to record the S K-edge and Fe K-edge absorption spectra of iron sulfides. The first multiple scattering calculation of the S K-edge absorption spectrum of FeS was performed by Kitamura, Sugiura, and Muramatsu.[6] The Fe K and $L_{2,3}$ and S K x-ray absorption edges have been recorded and are discussed in terms of the calculated band structures by Womes *et al.*[7] The S K-edge XANES of the $3d$ transition monosulfides VS, CrS, MnS, FeS, CoS, and NiS were recently investigated by Zajdel *et al.*[8] and compared with linear muffin-tin orbital (LMTO) numerical calculations. But very little attention in the literature has been given to the investigation of calcium, magnesium, and manganese sulfides.

Some of the physical properties of the studied sulfides cannot be explained without a detailed study of their electronic structure. The electronic structure of the valence band of many monosulfides has been widely investigated. In contrast, the electronic structure of the conduction band has received much less attention due to limitations of theoretical calculations and experimental approaches. Some experimental measurements carried out by different methods[9–13] have yielded information on aspects of the electronic structure of the investigated sulfides, for example, the experimental estimation of band gaps. But only theoretical methods yield a complete description of the electronic energy band structure. The electronic band structures of CaS, SrS, and BaS have been calculated by the method of linear augmented plane waves (LAPW).[14] The self-consistent Hartree-Fock method including correlation has been applied to compute the energy-band structure of MgS, SrS, and CaS, and the total density of occupied states in the valence band of MgS and SrS.[15] The band structure and the total density of states for MgS have been established by Stepanyuk *et al.*[16] based on the totally self-consistent linear augmented plane-wave method. The structure of sulfur p valence bands along high symmetry directions of the first Brillouin zone and total density only for occupied states of $B3$ and $B1$ crystal phases of MgS has been determined by Lichanot, Dargelos, and Larrieu using an *ab initio* Hartree-Fock linear combination of atomic orbital approach.[17] Band structures of alkali-earth-metal sulfides have been calculated by Ching, Gan, and Huang[18] using the self-consistent orthogonalized linear combination of atomic orbitals (OLCAO) method in the local density approximation (LDA). Kalpana *et al.*[19] used the tight-binding linear muffin-tin orbital (TBLMTO) method to determine the band structure of $B1$ and $B3$ phases of MgS and MgSe and to calculate the total density of states of the sulfides. Schematic band-structure models for MgS, CaS, and MnS were presented by Farrell *et al.*[20] It is necessary to note that in the above-mentioned papers only the total density of states of investigated compounds has been studied. Up to now the projected density of states (DOS) of the monosulfides were not obtained. In the present paper we re-

port the projected density of states in the conduction band of CaS and MgS calculated in the wide energy range.

There are several possible approaches for theoretical calculation of XANES spectra.[2,21,52] Calculations can be made by real-space multiple-scattering formalisms[22,43] or *k*-space (band-structure) codes used normally for DOS calculations.[23,24] Although modern band-structure methods are full potential (they do not use the muffin-tin approximation) and can incorporate the core-hole effect through a large supercell, their demands on computational resources are excessive and they are limited to a low-energy region above the x-ray absorption edge. Recently, several new methods have been tested for XANES simulations.[25,26] Application of the Bethe-Salpeter formalism[25] has not improved the existing agreement between theory and experiment. The finite-difference method[26] (FDM) is shown to be very expensive with respect to computing time and gives the same results for close-packed solids as the muffin-tin multiple-scattering theory. It improves agreement between theoretical and experimental XANES only for unpacked materials such as plane complexes. Thus, it was recommended in Ref. 26 that: "... the multiple scattering method should be used whenever possible ... and only in case of low symmetry, and when the discrepancy with experiment remains too important, the FDM should be used."

On the other hand, very recently, successful full multiple-scattering analysis of XANES in transition-metal oxides[27] and condensed zinc oxide (to high pressure[28]) have been reported. Based on the agreement between theory and experiment, it was concluded that nonspherical corrections do not appear to be significant for transition-metal oxides, except for very small variations in relative peak intensity within only a few eV above the edge. The results of Ref. 27 verified also that the ground-state DOS obtained within the full multiple-scattering approach using clusters of about 150 atoms are in good agreement with those of full-potential linear augmented plane-wave (LAPW) band structure calculation done with the WIEN code.[24] No evidence for multiplet-electron or sharp multielectron features due to many-body effects has been found in *K*-edge XANES spectra of transition-metal oxides.

In this study, we present experimental and theoretical XANES spectra near the sulfur *K* and $L_{2,3}$ edges of Mg, Ca, Mn, and Fe sulfides. Some initial theoretical analysis of sulfur *K*-edge XANES has been presented previously[20] for clusters limited to nine shells in size. It is necessary to note that the *L* edges of light elements such as sulfur, unlike the *K* edges, have not been widely studied. This is due to the fact that experiments in this low-energy region (100–1000 eV) are more difficult to perform because a high-vacuum system is required. In the literature, there are several studies in which the experimental and theoretical *K*-edge XANES spectra of sulfur are discussed.[29–31] But the S *L*-edge XANES spectra of CaS, MgS, and MnS have not been measured previously. The theoretical S $L_{2,3}$-edge XANES spectra of CaS, MgS, and MnS are calculated here.

We also study the local structure of a solid solution of iron and magnesium sulfides, which corresponds to the mineral niningerite ($Mg_{1-x}Fe_xS$). The experimental S *K*-edge XANES spectra of synthetic niningerite were obtained by Farrell and Fleet.[32] It is known that FeS has the NiAs-type ($B8$) structure under standard conditions. But it was found that FeS changes its local structure from NiAs-type ($B8$) phase to a new configuration influenced by the MgS matrix. It was suggested that this new iron sulfide phase was of NaCl-type ($B1$) structure. The solid solution $Mg_{1-x}Fe_xS$ has the homogenous rocksalt ($B1$) structure when $0<x<0.68$; at $x>0.68$ there are two-phase mixtures of $Mg_{0.32}Fe_{0.68}S$ ($B1$) and FeS ($B8$). The S *K*-edge XANES spectrum of the hypothetical cubic ($B1$) FeS phase was derived from the spectrum of $Mg_{0.375}Fe_{0.625}S$. One goal of the present investigation was to verify on the basis of a theoretical model that the local cubic configuration of iron sulfide really exists in the $Mg_{1-x}Fe_xS$ solid solution.

II. EXPERIMENT AND METHOD OF CALCULATION

All samples were prepared from high-purity elements by dry reaction within evacuated sealed silica glass tubes. CaS was prepared by direct reaction of crushed Ca metal and S, weighed to excess of the stoichiometric proportion, at 600 °C overnight and 800 °C for 1 h. The product was then ground and reloaded with excess S into a 20-cm-long sealed silica glass tube and heated in a horizontal tube furnace at 700 °C overnight and 800 °C for 1 h, maintaining a thermal gradient along the tube sufficient to allow any excess S to condense at the cool end. The CaS product was then reacted at 1000 °C for 3 days, then ground and annealed at 1000 °C for 4 days, reground and annealed at 1000 °C for 1 h, and quenched in water. MgS was prepared by direct reaction of Mg powder and S, weighed to a slight excess (~1 wt %) of the stoichiometric proportion, contained in a 6-mm-diam alumina crucible, which was set on a graphite pedestal within a sealed silica glass tube, and heated in a vertical tube furnace at 450 °C overnight, 600 °C for 1 day, 700 °C for 1 day, and 800 °C for 1 h. The MgS product was then reground, similarly loaded in a sealed silica glass tube with a slight excess (~1 wt %) of S, and then heated in the presence of graphite at 600 °C for 2 h, 900 °C for 2 h, and 1000 °C for 3 days. MnS was prepared by direct reaction of hydrogen-reduced (~800 °C) Mn powder and S, weighed to a slight excess of ~1 wt %, at 450 °C overnight, 600 °C for 2 days, and 700 °C for 1 h. Stoichiometric FeS (troilite) was prepared similarly by direct reaction of hydrogen-reduced (~900 °C) Fe sponge and a stoichiometric proportion of S at 450 °C overnight, 600 °C for 1 day, and 700 °C for 2 days.

Sulfur *K*- and *L*-edge XANES spectra were collected at the Canadian Synchrotron Radiation Facility (CSRF) and Aladdin storage ring (University of Wisconsin at Madison, Wisconsin). The storage ring operates at either 800 MeV or 1 GeV with a ring current of 60–180 or 40–80 mA, respectively; the XANES spectra were not markedly affected by differences in operating energy. The S *K*- and *L*-edge spectra were measured on a double-crystal monochromator (DCM) beam line and a Mark IV Grasshopper monochromator beam line, respectively, in both total electron yield (TEY) and fluorescence yield (FY) modes as a function of incident photon

energy;[33] both beam lines actually collect the current yield (CY) but this has traditionally been referred to as ''TEY.'' The DCM is described by Yang *et al.*[34] and uses an InSb(111) crystal with an energy resolution of about 0.6 eV [full width at half maximum (FWHM)] at 1840 eV; the Darwin width of the crystal corresponds to an energy resolution of 0.9 eV for the S *K* edge. The Grasshopper beam line is described by Tan *et al.*[35] and uses an 1800 line/mm holographic grating with an energy resolution of ~0.1 eV in the S *L*-edge region. The superior resolution at the S *L* edge is attributed to inherently narrower natural linewidths and narrower photon widths due to use of a low-energy grazing-incidence monochromator.

The TEY recording mode probes the near surface (estimated at <100 Å depth for the *K* edge and <50 Å depth for the *L* edge) and is sensitive to near-surface impurities and alteration, whereas the FY mode is more representative of the bulk material (i.e., >1000 Å depth for the *K* edge and ~100 Å depth for the *L* edge[36,37]). Thus, collection of spectra in both the TEY and FY modes simultaneously for the same sample, and particularly for the *L* edge, provides information on near-surface homogeneity and structural continuity. Transmission measurements have not been made in the XANES region on the DCM or Grasshopper beam lines. For XANES spectroscopy, differences between TEY and FY modes are attributed to bulk sensitivity and scaling only. However, for extended x-ray fine-structure (EXAFS) spectroscopy, which is not presently investigated, differences in amplitude between TEY and FY modes can introduce small differences in measured bond lengths.

The grain size of the samples was <0.3 mm in diameter; therefore, individual crystals were far too small to cleave. For both *K*- and *L*-edge studies, the sample was crumbled, if necessary, but not ground, and uniformly distributed on double-sided conducting carbon tape affixed to a clean stainless-steel disk. For the *K*-edge XANES, the sealed silica glass sample tubes were opened in air immediately before measurement. However, the relatively high reactivity of the metal sulfides and the near-surface sensitivity of the *L*-edge measurements made it essential to collect the *L*-edge spectra on samples with minimal exposure to air and moisture. Therefore, for *L*-edge measurements, sample preparation, including opening of the sample tubes, and transfer into the experimental chamber of the Grasshopper were performed in a nitrogen-filled glove bag attached to the port of the spectrometer sample chamber.

DCM (*K*-edge) measurement conditions included a photon energy range of 2450–2525 eV at a step size of 0.25 eV, with count times determined by counting statistics (~3.3 s per step), and 2 scans per sample, giving a total run time of approximately 27 min per sample. The Grasshopper (*L*-edge) measurement conditions included a photon energy range of 155–190 eV at a step size of 0.07 eV, with a count time of 1 s per step and 4 scans per sample, giving a total run time of approximately 40 min per sample. Data reduction and analysis used the BAN and BGAUSS data analysis programs[38] and FORTRAN77 codes. *L*-edge spectra were normalized against incident intensity (I_0), which was measured simultaneously. Both TEY and FY modes of *L*-edge spectra yielded similar spectral features, but the TEY spectra are currently used for presentation and interpretation due to their more favorable signal-to-noise ratio. All spectra were calibrated to the *K*- or L_3-edge peak of native S at 2472.0 and 162.5 eV ($2p_{3/2}$),[39,40] respectively, after removal of a linear preedge background. To discern relative changes in subtle XANES features, all spectra were scaled relative to the maximum peak height at the edge. S *K*- and *L*-edge spectra for native S were collected at the beginning of each beam time session for calibration purposes and showed excellent agreement with respect to relative position and intensity of spectral features.

Our S *K*-edge XANES spectra of labeled sulfur compounds, including metal sulfides, compare very favorably with measurements on Si(111) monochromator beam lines (e.g., Refs. 41 and 42). This is because the core-hole lifetime broadening is significantly greater than the resolution of the Si(111) crystal. Also, the edge feature (or white line) of the XANES spectra is considerably broadened by fine structure reflecting complexity in the final states. We emphasize that no new features are evident in S *K*-edge XANES spectra of metal monosulfides recorded using a Si(111) monochromator.

The computer code[43] G4XANES was used in the present calculations. The algorithm of the full multiple-scattering method was described earlier.[43] Atomic charge densities were obtained with the help of a self-consistent Dirac routine. Phase shifts of the photoelectron were calculated in the framework of the crystal muffin-tin (MT) potential scheme with touching MT spheres. The MT radii and the MT constants were obtained according to an established procedure of MT potential construction.[43] The MT approximation according to the Mattheiss prescription[44] with Slater exchange ($\alpha = 1.0$) was used while constructing the crystal potential. This approach was successfully applied recently for the analysis of XANES in various compounds.[45–47]

For comparison purposes, we made calculations of the S *K*-edge XANES of MgS and FeS ($B8$ phase) using the FEFF8.2 package[22] based on the self-consistent Hedin-Landquist potential, with results very close to those obtained by our method, except for slightly larger broadening in the high-energy region of the XANES spectra for FEFF8.2.

It is well known[48] that within the dipole approximation the x-ray absorption coefficient $\alpha(E)$ for the S *K* edge is given by

$$\alpha(E) = |m_L(E)|^2 N_p^S(E), \tag{1}$$

where $N_p^S(E)$ is the partial density of unoccupied S states with p symmetry and $m_L(E)$ is the normalized dipole transition matrix element given by

$$m_L(E) = \frac{\int dr\, \Phi_l(r,E)\Delta(r)\Psi_c(r)}{\left[\int dr\, \Phi_l^2(r,E)\right]^{1/2}}, \tag{2}$$

where $\Phi_l(r,E)$ is a solution of the radial Schrodinger equation at energy E for the MT potential ($l=1$ for the *K* edge), $\Delta(r)$ is the electron-photon interaction operator, and $\Psi_c(E)$

is the core *K*-level wave function. In the calculation, phase shifts with orbital momentum (l) up to 3 have been included.

For the S $L_{2,3}$-edge XANES, the situation is more complicated. There are two dipole-allowed channels ($p \rightarrow d$ and $p \rightarrow s$). We have calculated the S L_3 edge as a sum of partial $p \rightarrow s$ and $p \rightarrow d$ cross sections. The S $L_{2,3}$ edge has been obtained as a superposition of the S L_2 and S L_3 shifted by the value of spin-orbit splitting of 1.1 eV. It is well known that the spin-orbit interaction changes the L_2/L_3 branching ratio for several transition-metal $L_{2,3}$ edges from 1:2 (see, for example Ref. 49), and several theoretical approaches have been suggested to estimate this ratio theoretically.[50,51] But according to our knowledge there is no indication in the literature of a significant deviation of the branching ratio from 1:2 for the sulfur $L_{2,3}$ edge. That is why (as the exact value of the branching ratio for the S $L_{2,3}$ edges in the compounds under the study is not known) we tried the 1:2 ratio (L_2:L_3) with quite reasonable results for the superimposed sulfur L_2 and L_3 edges.

In order to perform a direct comparison with experimental data one must take into account two factors. One factor is the filling of the occupied states following the Fermi distribution. The other factor is the broadening of experimental spectra due to the core-hole lifetime, the finite mean free path of the photoelectron, and the experimental resolution. For the bandwidth of the core hole, we used 0.59 eV for the S *K*-edge XANES and a 0.05 eV for the S $L_{2,3}$-edge XANES. The energy-dependent function obtained by Muller, Jepsen, and Wilkins[48] was used for the mean free path of the photoelectron. The experimental energy resolutions are 0.9 for S *K*-edge XANES and ~0.1 eV for the S $L_{2,3}$-edge XANES. All these factors contribute to the imaginary part of a complex MT potential.

In addition, one must compare the experimental data with the theoretical calculation made using a relaxed potential (i.e., taking into account the presence of the core hole). This effect was treated in the $Z+1$ approximation.[52] We found that for the *K* edge the contribution of the core hole is rather small, while for the S $L_{2,3}$ edge, the core-hole effect is more important.

III. RESULTS AND DISCUSSION

A. Sulfur *K* edge of MgS, CaS, and MnS

A first step in the multiple-scattering analysis of XANES data is the determination of the minimum size of the cluster of neighbor atoms around the absorbing S atom, within which the scattering of the photoelectron can reproduce the entire fine structure of the XANES. So, the comparison of the experimental S *K*-edge XANES spectra of MgS with the theoretical simulations carried out for different sizes of cluster was undertaken. Good agreement between theoretical and experimental spectra is reached for the comparatively large cluster containing nine coordination shells. The comparison of the experimental and theoretical S *K*-edge XANES spectra of MgS is shown in Fig. 1. The scale is utilized for convergence in comparing the experimental data with the calculated spectra, where the zero value of the muffin-tin energy is chosen as the origin of the energy scale. The spectra were aligned relative to the position of peak *A*.

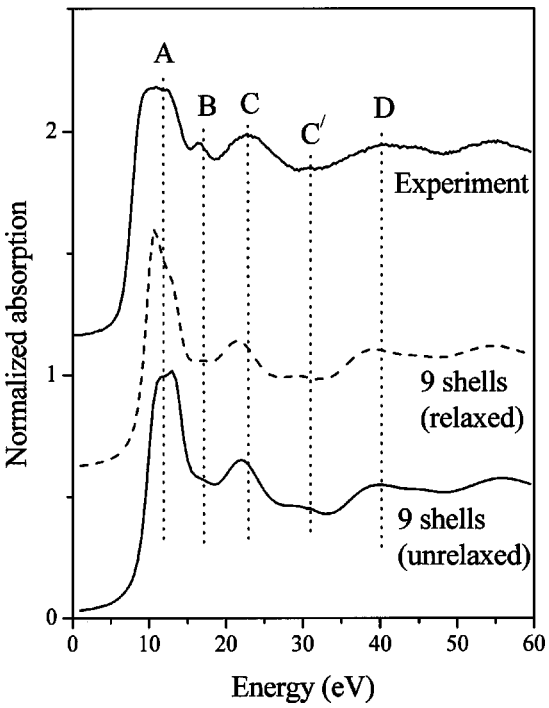

FIG. 1. Comparison of experimental S *K*-edge XANES for MgS with theoretical XANES spectra calculated for the cluster of nine shells (147 atoms). The theoretical spectra were calculated in both ground-state potential (solid line) and fully relaxed potential using the $Z+1$ approximation (dashed line). The broadening factors and Fermi distribution were taken into account in the calculations.

It was discussed earlier [see Eq. (1)] that in the dipole approximation the transition rate of x-ray absorption (for example, at the S *K* edge) is proportional to the transition matrix element and projected *p* density of sulfur unoccupied states. An important difference between the calculation of the density of states and the x-ray absorption spectra lies in the fact that, for the density of states, one needs to use the ground-state potential of the electronic system, whereas for the x-ray absorption case one needs to use the potential of the excited state, because the absorbing atom is no longer in the ground state. However, in this study it was found that the spectrum calculated within a potential of the core hole using the $Z+1$ approximation (dashed line in Fig. 1) does not give better agreement with the experimental spectrum compared with the spectrum calculated within the ground-state potential. This finding means that one can use the experimental x-ray absorption spectra to study unoccupied electronic states in the conduction band, if the transition matrix element is a smooth function of the energy. This is the case for the S *K*-edge XANES spectrum of MgS. Thus, the shape of the experimental S *K*-edge XANES of MgS can be used to study of the *p* density of sulfur unoccupied states of MgS.

In Fig. 2(a) the experimental and theoretical S *K*-edge XANES spectra of calcium sulfide are presented. The theoretical spectrum is calculated in the ground-state potential for an atomic cluster size of 251. It was found that the spectrum

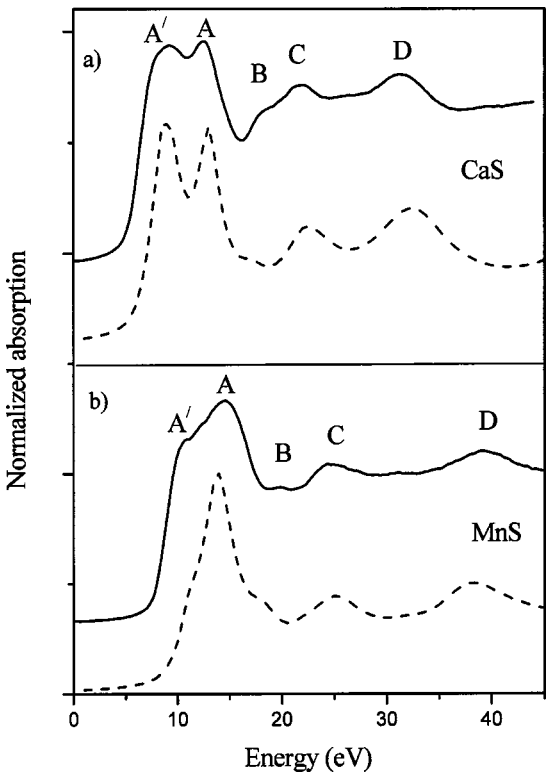

FIG. 2. Comparison of experimental S K-edge XANES for (a) CaS and (b) MnS with theoretical XANES spectra for a 13 shell (251 atom) cluster. The theoretical spectra were calculated in ground-state potential. The broadening factors and Fermi distribution were taken into account in the calculations.

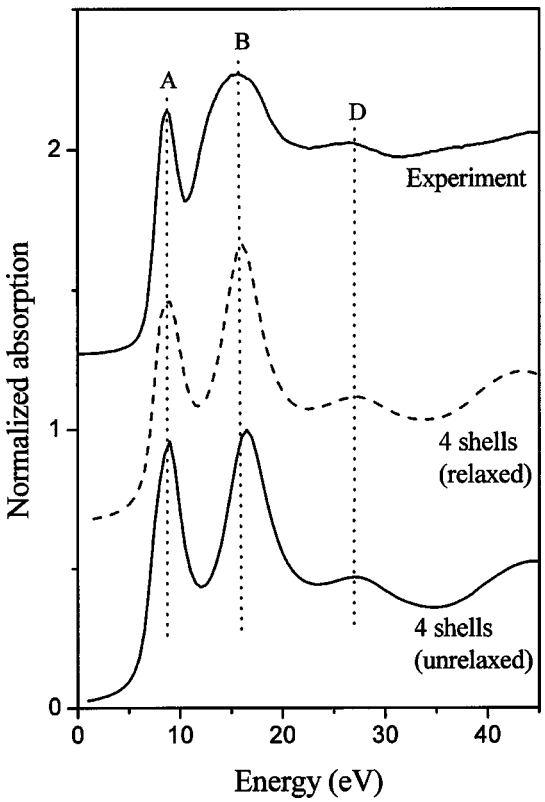

FIG. 3. Comparison of experimental S K-edge XANES for FeS (B8 phase) with theoretical XANES spectra calculated in ground-state potential (solid line) and fully relaxed potential using the $Z+1$ approximation (dashed line). The cluster size of four shells (37 atoms) was used to calculate spectra. All of the broadening factors and Fermi distribution were taken into account in the theoretical spectra.

calculated for a cluster size of 13 shells is in better agreement with experiment with respect to the relative intensity of peaks A and A' as compared with the spectrum calculated for a cluster of nine shells. Therefore, we conclude that the XANES spectrum for the S K edge in CaS results from the multiple scattering of an excited photoelectron inside a large cluster of 13 shells (251 atoms). The comparison of the experimental S K-edge XANES spectrum of MnS with the theoretical simulations calculated in the ground-state potential for an atomic cluster size of 251 is shown in Fig. 2(b). It was found that optimum agreement between the experimental S K-edge XANES of MnS and our theory also requires a cluster size of at least 13 shells (251 atoms). Thus, for cubic crystals having large number of colinear atomic chains (MgS,CaS,MnS) one needs to take into account many atomic shells (up to 13) for XANES calculations. This finding is confirmed by results of previous calculations for other cubic structures.[2]

B. Local atomic geometry of iron sulfide

It is well known that iron sulfide, unlike magnesium, calcium, and manganese sulfides, has NiAs-type structure at ambient pressure and temperature. However, when the structure of the $Mg_{1-x}Fe_xS$ solid solution was studied[32] it was found that the configuration of iron sulfide changed to another type at $x=0.68$. The S K-edge XANES spectrum of the hypothetical cubic ($B1$) FeS phase has been derived from the spectrum of $Mg_{0.375}Fe_{0.625}S$ by Farrell and Fleet.[32] In the present research, theoretical analysis of XANES spectra was used to study the changes of local structure around sulfur atoms in the $Mg_{1-x}Fe_xS$ solid solution. We have calculated the theoretical S K-edge XANES spectrum of FeS in the $B1$ phase in order to show that NaCl-type ($B1$) phase of iron sulfide really exists in the $Mg_{1-x}Fe_xS$ solid solution. We also present the comparison of the S K-edge XANES spectra of iron sulfide in both $B8$ and $B1$ phases in order to establish the changes that occur in the S K-edge XANES spectrum when the structural transition takes place.

In the process of calculations it was found that the XANES spectrum for the S K edge in FeS ($B8$) results from the multiple scattering of an excited photoelectron inside a relatively small cluster of four shells (37 atoms). In Fig. 3 we present the theoretical sulfur K-edge XANES of FeS ($B8$) calculated in both the ground-state potential (unrelaxed) and the $Z+1$ approximation (fully relaxed). The experimental S K-edge XANES of FeS ($B8$) is also shown in Fig. 3. Evidently, the theoretical S K-edge XANES calculated for the ground-state potential and fully relaxed potential do not differ significantly (although the spectrum calculated in the $Z+1$ approximation agrees slightly better with the experimental one in the relative intensity at peak positions).

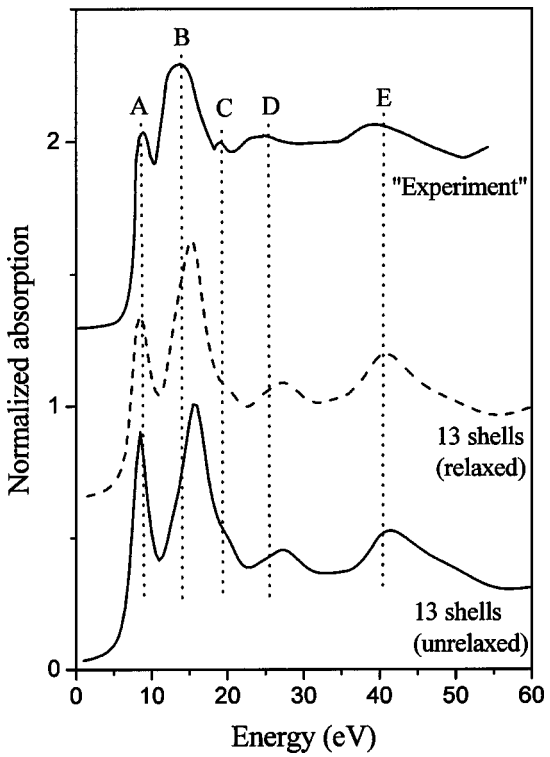

FIG. 4. Comparison of experimental S *K*-edge XANES of rocksalt FeS (B1 phase) with theoretical XANES spectra calculated for the cluster size of 13 shells (251 atoms). The dashed line corresponds to the fully relaxed potential calculation ($Z+1$ approximation); solid line to the ground-state potential calculation.

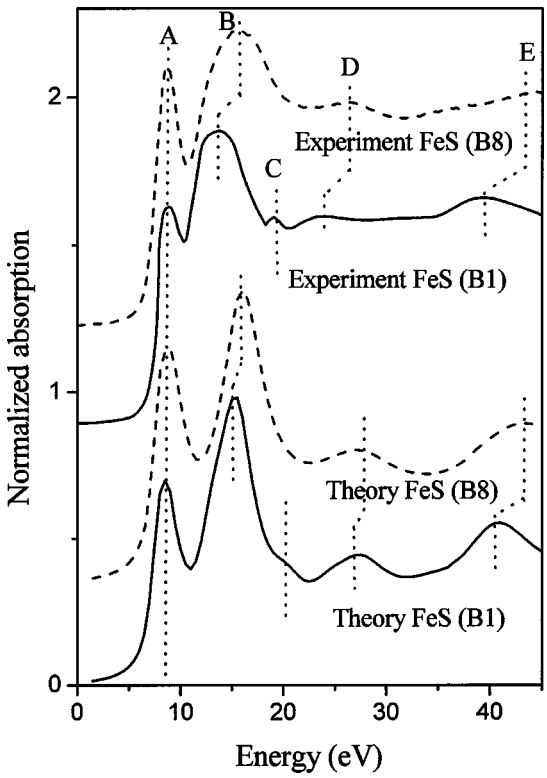

FIG. 5. Comparison of experimental S *K*-edge XANES for both rocksalt (B1) FeS and NiAs-type (B8) FeS with theoretical relaxed spectra. Dashed lines correspond to B8 structure of FeS solid lines to B1 structure.

In Fig. 4 we compare the experimentally derived S *K*-edge XANES spectrum of FeS (Ref. 32) (rocksalt; *B*1 phase) with theoretical spectra calculated for a cluster size of 13 coordination shells (251 atoms). It was established that good agreement between theoretical and experimental spectra of NaCl-type FeS takes place only for a large cluster of nine shells or larger because the theoretical spectrum reproduces peak *C* only when the number of coordination shells in the cluster reaches nine. The calculation taking into account the fully relaxed potential does not differ from XANES calculated in ground-state potential (Fig. 4).

In Fig. 5, we compare the experimental S *K*-edge XANES spectra for *B*1 and *B*8 phases of FeS with theoretical simulations. The spectra were aligned relative to the position of peak *A*. One can see that the intensity of peak *A* of the *B*1 phase spectrum is smaller compared with the spectrum of the *B*8 phase of FeS. The same behavior is observed in the theoretical spectra. The peaks *B*, *D*, and *E* of the *B*1 phase shift in the low-energy region relative to the *B*8 phase. This displacement occurs in both experimental and theoretical spectra. The experimental XANES spectrum of the *B*1 phase has a peak marked as *C*, but this detail is absent in the experimental spectrum of the *B*8 phase. The same behavior is observed for the theoretical XANES spectra.

Thus, we have obtained good agreement between ''experimental'' and theoretical S *K*-edge XANES spectra of *B*1 phase iron sulfide. So, the results of the present theoretical investigation confirm the hypothesis[32] that the iron sulfide changes its configuration from NiAs-type (*B*8) to NaCl type in $Mg_{1-x}Fe_xS$ solid solution under the influence of MgS at a concentration of iron ions (x) below 0.68. More detailed discussion of this phenomenon can be found elsewhere.[53,54]

C. $L_{2,3}$ edge of sulfur

In this paper we present experimental and theoretical XANES spectra near the S $L_{2,3}$ edge of metal monosulfides. The S *L* edge is located at 162.5 eV, and is split by 1.1 eV due to the spin-orbit interaction. According to dipole selection rules, the electronic transition corresponding to S $L_{2,3}$ XANES includes two $\Delta l=\pm 1$ channels: $p\rightarrow d$ and $p\rightarrow s$. We present S $L_{2,3}$-edge XANES spectra in all studied compounds calculated as the sum of two dipole-allowed channels. However, because of a small relative value of the transition matrix element for the $p\rightarrow s$ channel in the near-edge energy region, the contribution of the $p\rightarrow s$ partial cross section to the total S $L_{2,3}$ XANES spectrum of MgS, CaS, MnS, and FeS was found to be almost negligible. As an example in Fig. 6 we report the calculations for two partial cross sections ($p\rightarrow d$ and $p\rightarrow s$) corresponding to the S L_3-edge XANES in CaS.

In Fig. 7 the comparison of the experimental S $L_{2,3}$-edge XANES in MgS with the theoretical XANES spectra is reported. The spectra were aligned in energy relative to the position of peak *A*. In the process of making the calculations it was established that the S $L_{2,3}$ edge in MgS results from

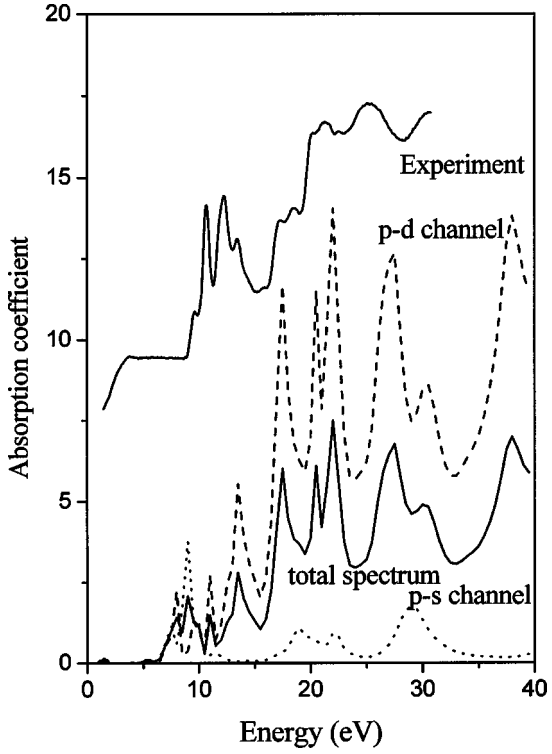

FIG. 6. Calculated cross section for S $2p \rightarrow 3d$ and S $2p \rightarrow 4\varepsilon s$ transitions for the large size cluster (13 shells) in the ground-state potential of CaS. The dashed line corresponds to the S $2p \rightarrow 3d$ transition, and the dotted line to the S $2p \rightarrow 4\varepsilon s$ transition. The total S L_3-edge XANES spectrum of CaS calculated with consideration of both S $2p \rightarrow 3d$ and S $2p \rightarrow 4\varepsilon s$ channels and the experimental spectrum are also shown.

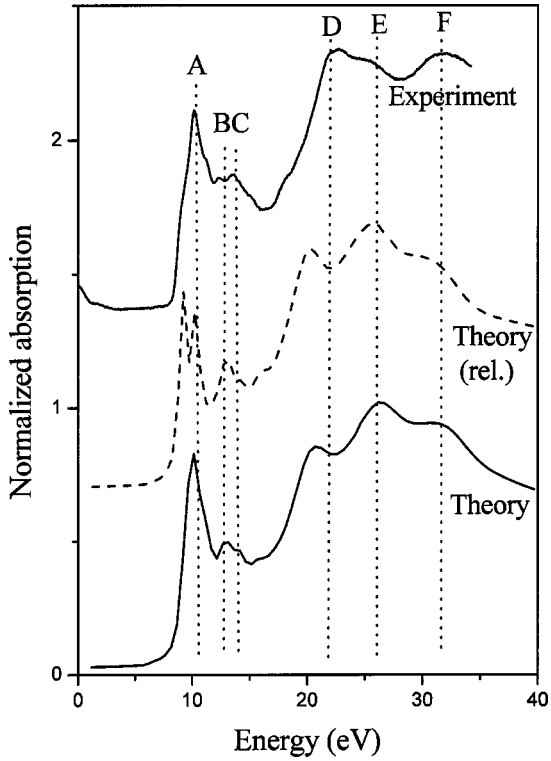

FIG. 7. Comparison of experimental S $L_{2,3}$-edge XANES for MgS with theoretical XANES spectra calculated in both ground-state potential and relaxed potential (dashed line). The theoretical spectra were calculated taking into account all of the broadening factors and Fermi distribution.

the multiple scattering of an excited photoelectron inside a large cluster of nine shells (147 atoms). It is shown that the spectrum calculated in the $Z+1$ approximation (dashed line in Fig. 7) is in poorer agreement with the experimental one (the first peak A of the theoretical spectrum calculated in the relaxed potential is split while peak A of the experimental spectrum is not split).

In Fig. 8 the experimental S $L_{2,3}$ edge of CaS has been compared with the theoretical full multiple-scattering simulations. In the case of the S $L_{2,3}$ edge of CaS it is found that the spectrum calculated using the $Z+1$ approximation (see dashed line) agrees better with experiment in the energy position of peaks than that calculated in ground-state potential. The S $L_{2,3}$-edge XANES spectrum of CaS was calculated for different cluster sizes. It was established that all main details of the experimental spectra are described by a large cluster containing 13 shells (251 atoms).

Figure 9 compares the experimental sulfur $L_{2,3}$-edge x-ray absorption spectrum of MnS and theoretical spectra calculated in both fully relaxed potential (dashed line) and ground-state potential. The spectra are aligned relative to the position of peak E. In the process of the calculations it was found that a large cluster of 13 shells (251 atoms) is needed to reproduce all details of the experimental S $L_{2,3}$-edge XANES in MgS. It is evident that the calculations carried out with a ground-state potential are in poorer agreement with the experimental S $L_{2,3}$-edge XANES spectrum than those carried out with the core-hole potential.

Figure 10 shows the comparison of the experimental S $L_{2,3}$-edge XANES spectrum of $B8$ phase FeS with theoretical calculations. Only two features (A and D) can be seen in the spectrum for a cluster consisting of 1 shell (7 atoms). The cluster of 2 shells (19 atoms) reproduces all fine details (A,B,C,D,E) of the experimental XANES, but it does not agree well with experiment in the intensity of the first peak A. Including four shells (37 atoms) in the calculation results in good agreement with the experiment in respect to peak position and intensity. The calculation with the $Z+1$ approximation (dashed line in Fig. 10) does not change the shape of the experimental XANES significantly.

D. Density of states

The studied monosulfides have attracted attention as compounds with a large diversity of physical properties related to their energy band structure. Attempts to understand the electronic structure of the metal sulfides were made earlier by different theoretical methods. Analysis of the electronic band structure of magnesium sulfide predicts an indirect (Γ-X) band gap.[15,16,19] In materials with an indirect band gap the bottom of the conduction band and the top of the valence band lie at different wave vectors. The band gap in MgS is bounded by S p states in the upper part of the valence band[15,16,19] and Mg s states[16,19] (and to a less extent, S d) in

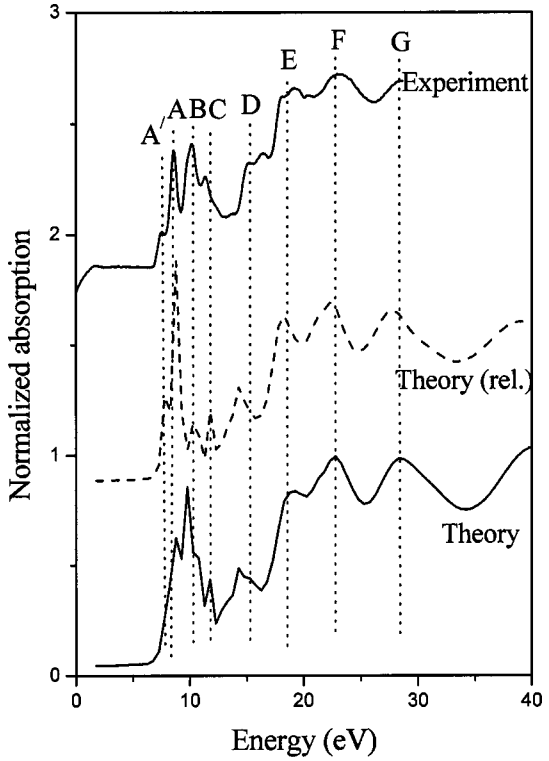

FIG. 8. Comparison of experimental S $L_{2,3}$-edge XANES for CaS with theoretical XANES spectra calculated in both ground-state potential and fully relaxed final-state potential (dashed line). The theoretical spectra were calculated taking into account all of the broadening factors and Fermi distribution.

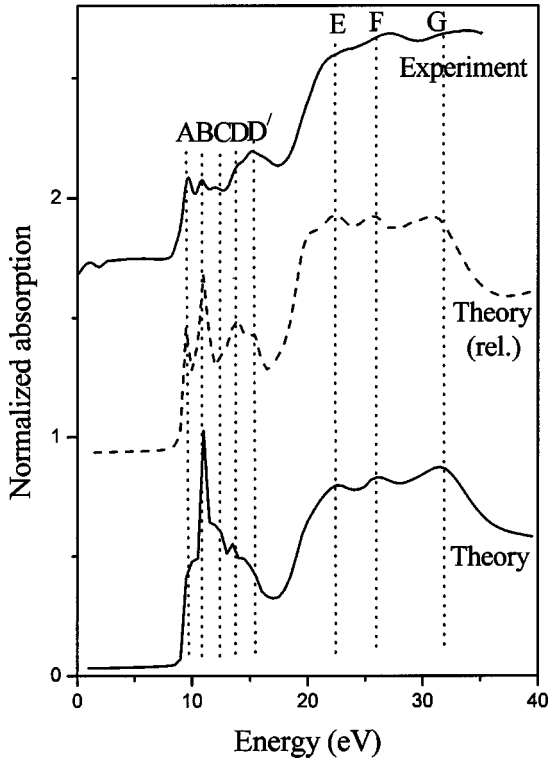

FIG. 9. Comparison of experimental S $L_{2,3}$-edge XANES for MnS with theoretical XANES spectra calculated with the ground-state potential and fully relaxed potential (dashed line). The theoretical spectra were calculated taking into account all of the broadening factors and Fermi distribution.

the conduction band. Different estimates of the band gap width of MgS are given in the literature. Stepanyuk *et al.*[16] using the totally self-consistent linear augmented plane-wave method have found that the value of the band-gap width is 2.69 eV. This result is in a good agreement with that calculated by Kalpana *et al.*[19] (2.7 eV) using the tight-binding linear muffin-tin orbital (TBLMTO) method. But the Hartree-Fock calculation performed by Pandey *et al.*[15] has resulted in band-gap value of 6.48 eV. Ching, Gan, and Huang[18] based on the OLCAO method have determined that the gap width of MgS is equal to 4.59 eV.

In CaS the band gap [estimated variously as 2.143 eV,[14] 3.2 eV,[18] or 7.6 eV (Ref. 15)] lies between the S *p* states[14,15] in the valence band and Ca *d* states[14] in the conduction band. Pandey *et al.*[15] disagree with the view of Stepanyuk *et al.*[14] and Ching, Gan, and Huang[18] that CaS is an indirect (Γ-X) band dielectric. It is claimed[15] that CaS is a direct-band-gap material.

Moreover, several experimental measurements of band gaps in magnesium and calcium sulfides have been carried out. X-ray photoelectron spectroscopy (XPS) measurements on bulk MgS and ZnSe/MgS superlattice made by Suzuki *et al.*[9] indicate that the band-gap width of MgS is 5.27–5.47 eV. Investigation of CaS single crystals by optical reflectivity and luminescence[10,11] resulted in an estimated indirect band-gap width of 4.434 eV, a direct gap (X) of 5.343 eV, and a direct gap (Γ) of 5.80 eV. Optical absorption measurements in CaS evaporated thin films[12] yielded a band gap width equal to 5.38 eV. CaS:Eu^{2+}:Sm^{3+} thin films were studied by Zhang *et al.*,[13] and a band gap equal to 4.48 eV was obtained. Thus, we can conclude that the experimental measurements of band-gap width differ from the theoretical estimations. Overall, the experimental band gaps are significantly larger than the theoretical gaps. The above-mentioned theoretical results were obtained by analyzing the band-structure calculations and densities of states of studied compounds. But in the literature we can find only total DOS calculations for occupied[14,15,17,19] or unoccupied states[14,19] of MgS and CaS. The projected DOS of investigated sulfides has not been computed.

In this paper we present curves proportional to the projected electronic densities of unoccupied states in the conduction band of MgS and CaS, which can be used in the first approximation as a draft scheme for the DOS in the compounds under study. In Fig. 11 the partial DOS in the conduction band of MgS are shown. It is seen that S *p* states lie at the top of the valence band of MgS. The bottom of conduction band is formed by Mg *s* states and S *s* states. Our calculations permit an estimated band-gap width for MgS of about 4.6 eV, although this value is only approximate. Recent studies of ZnS band structure clearly indicate that a better estimation of the band-gap width requires a more sophisticated approach like that of *GW*.[55] In Fig. 12 the partial densities of states in the conduction band of CaS are presented. It shows that the bottom of the conduction band is mainly

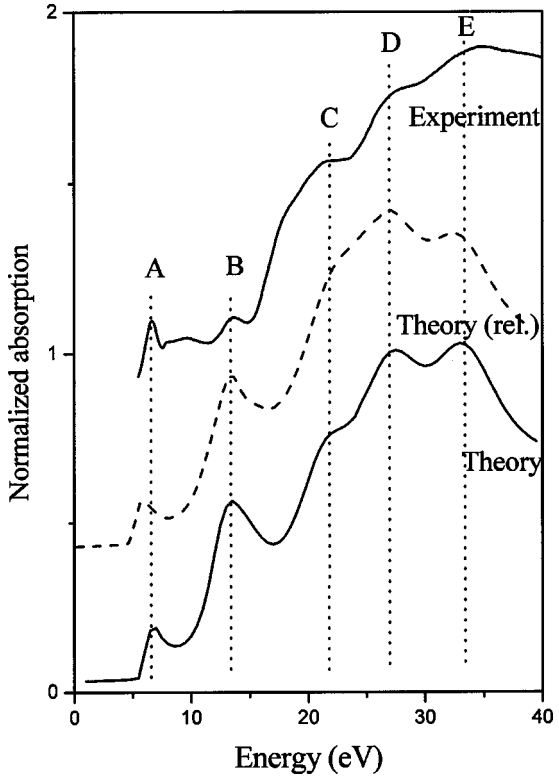

FIG. 10. Comparison of experimental S $L_{2,3}$-edge XANES for FeS (B8 phase) with theoretical XANES spectra calculated in both ground-state potential and fully relaxed potential (dashed line). The theoretical spectra were calculated taking into account all of the broadening factors and Fermi distribution.

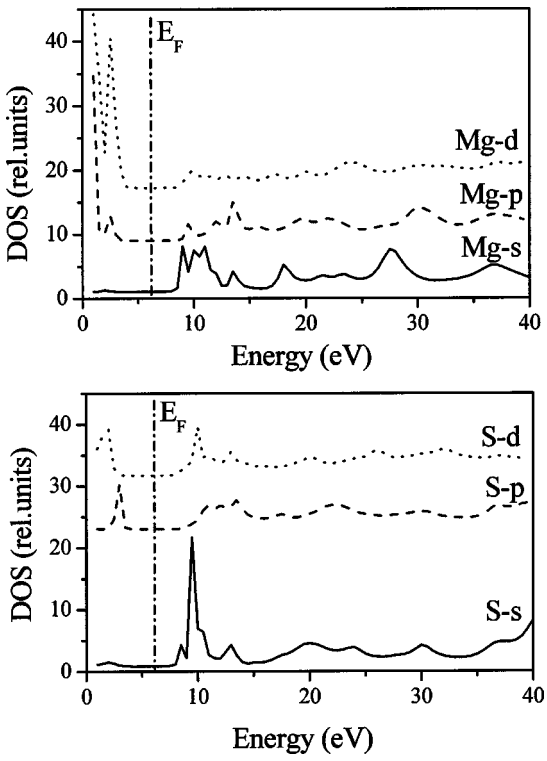

FIG. 11. Partial densities of unoccupied states in the conduction band of MgS, using a cluster of 13 shells (251 atoms). Origin of the energy scale corresponds to the zero of the MT potential. The vertical dash-dotted line locates the Fermi level.

formed by sulfur states (S d and s states and, in lower degree, S p states). We estimate that the band-gap width of CaS is about 3.5 eV.

The analysis of electronic structure of MgS and CaS explains why K- and $L_{2,3}$-edge XANES spectra of MgS differ from the corresponding spectra of CaS. It is known that the configuration of external electronic orbit of magnesium is $3s^2$ and that of calcium is $4s^2$. Thus, the electronic configurations of Mg and Ca differ only in main quantum number. Therefore, one might suppose that the S K-edge XANES spectra of CaS and MgS will be similar. Moreover, according to Natoli's rule (Bianconi[2]) for solids of the same crystal structure type, there is a simple relation between lattice spacing R and relative energy of corresponding XANES peaks, ΔE, namely $R^2\Delta E=$const. Thus, if one rescales the energy scale of CaS XANES by the factor $k=(R_{\mathrm{MgS}}/R_{\mathrm{CaS}})^2=0.83$ the resulting spectrum should be identical to the spectrum of MgS, if both compounds have the equivalent electronic structure. As one can see from Fig. 13 this is not the case, because the strong peak A' in the low-energy region of CaS sulfur K-edge XANES is not present in the MgS XANES. (There are also changes in the high-energy region of the CaS spectrum in comparison with the MgS spectrum.) To analyze why Natoli's rule cannot be applied to the CaS-MgS pair of compounds one needs to compare Figs. 11 and 12 where we present curves proportional to the local projected DOS of these compounds. Comparison of the two figures clearly indicates that the main reason for the prominent difference in the low-energy part of the sulfur K-edge XANES is the appearance of the maximum in Ca $3d$ unoccupied states in the energy region close to the bottom of conduction band of CaS.

For magnetic solids it is possible to apply a special kind of x-ray absorption spectroscopy in a magnetic field using the polarized nature of synchrotron radiation to measure the so-called XMCD spectra.[56] From these spectra one can extract information on spin-dependent characteristics of matter. A second technique to obtain spin-dependent XANES was proposed by Hamalainen *et al.*[57] (and analyzed theoretically, for the first time, by Soldatov *et al.*[58]), but this method is seldom used because of the very low intensity of this type of experiment. Spin-polarization effects are not detected by the conventional x-ray absorption spectroscopy used in this study. However, we have performed spin-dependent calculations of the local DOS (LDOS) for one of the compounds in our study, FeS ($B8$ phase), using the FEFF8.2 package and found that, except for Fe d states (and slight modifications of S p states), there is almost no shift in energy of the corresponding LDOS (see Fig. 14). An interesting effect can be seen in Fig. 14: in both spin-up and spin-down panels the position of the maximum of iron d states (dashed vertical lines) correspond to a minimum in the sulfur p states. Thus, one may say that the S p states are ''squeezed out'' of the energy positions of Fe d states, as a result of the specific interaction between iron and sulfur electronic states. For the unoccupied states such a specific interaction between elec-

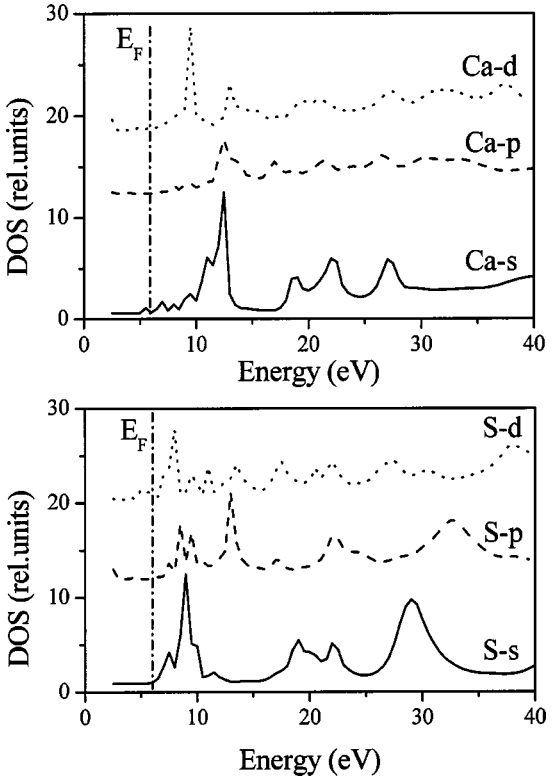

FIG. 12. Partial densities of unoccupied states in the conduction band of CaS, using a cluster of 13 shells (251 atoms). Origin of the energy scale corresponds to the zero of the MT potential. The vertical dash-dotted line locates the Fermi level.

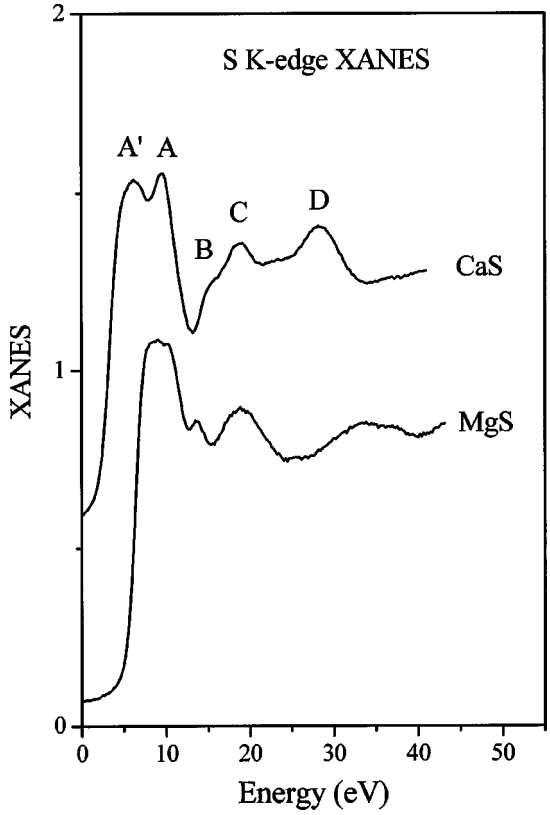

FIG. 13. Sulfur *K*-edge XANES in CaS and MgS scaled in energy according to Natoli's rule (see text).

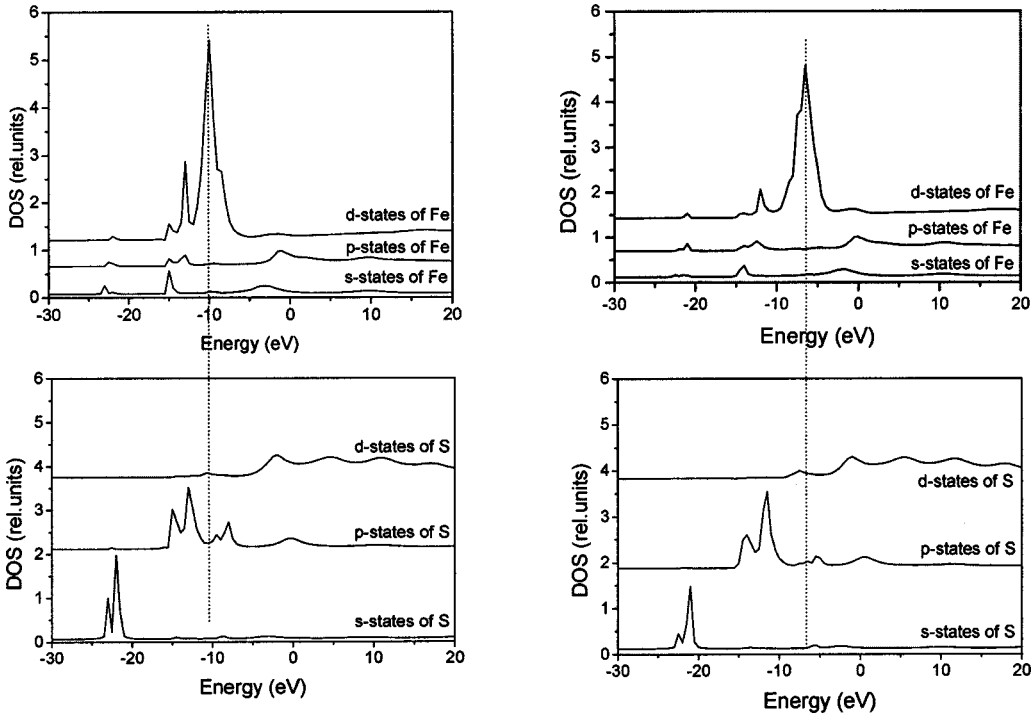

FIG. 14. Spin-polarized density of unoccupied states for FeS (B8 phase) calculated using FEFF8.2 (Ref. 22) package. Left panels are spin-up DOS, right panels are spin-down DOS.

tronic states has been previously found for rare-earth-metal sulfides,[59] CeO_2,[60] orthoferrites,[61] and stishovite.[62] Thus, one may conclude that in this energy region the interaction between S p states and Fe d states in the conduction band of FeS ($B8$) has repulsive character.

IV. CONCLUSIONS

We have applied a full multiple-scattering scheme for theoretical analysis of XANES in several monosulfides, obtaining theoretical S K- and $L_{2,3}$-edge XANES of MgS, CaS, MnS, and FeS. It is shown that good agreement between theoretical and experimental spectra is reached for a comparatively small cluster of about 40 atoms for the NiAs-type structure of FeS, although a larger cluster consisting of about 150–250 atoms is required for NaCl-type structures (MgS, CaS, and MnS). The shape of the experimental S K-edge XANES can be used to study the density of sulfur unoccupied p states of investigated sulfides. It was found that in $Mg_{1-x}Fe_xS$ solid solution iron sulfide changes its local structure from NiAs type ($B8$) to rocksalt type ($B1$), influenced by the MgS matrix. It is shown that Mg s and S s states lie at the bottom of the conduction band of MgS while Ca d and S d, s, and p states form the lower part of the conduction band of CaS. A special kind of repulsive interaction between unoccupied S p states and Fe d states has been found for $B8$ phase FeS, where S p states are squeezed out of the energy region of the Fe d states.

*Author to whom correspondence should be addressed. Email address: soldatov@rsu.ru

[1] M. E. Fleet and N. D. MacRae, Geochim. Cosmochim. Acta **51**, 1511 (1987).
[2] A. Bianconi, in *X-Ray Absorption: Principles, Applications and Techniques of EXAFS, SEXAFS and XANES*, edited by R. Prins and D. C. Koningsberger (Wiley, New York, 1988), p. 573.
[3] C. Sugiura, Y. Gohshi, and I. Suzuki, Phys. Rev. B **10**, 338 (1974).
[4] C. Sugiura, J. Chem. Phys. **74**, 215 (1981).
[5] C. Sugiura, J. Chem. Phys. **80**, 1047 (1984).
[6] M. Kitamura, C. Sugiura, and M. Muramatsu, Solid State Commun. **67**, 313 (1988).
[7] M. Womes, R. C. Karnatak, J. M. Esteva, I. Lefebvre, G. Allan, J. Olivier-Fourcade, and J. C. Jumas, J. Phys. Chem. Solids **58**, 345 (1997).
[8] P. Zajdel, A. Kisiel, M. Zimnal-Starnawska, P. M. Lee, F. Boscherini, and W. Giriat, J. Alloys Compd. **286**, 66 (1999).
[9] H. Suzuki, H. Nashiki, M. Hoshiyama, and I. Suemune, Nonlinear Opt. **18**, 227 (1997).
[10] Y. Kaneko and T. Koda, J. Cryst. Growth **86**, 72 (1988).
[11] Y. Kaneko, K. Morimoto, and T. Koda, J. Phys. Soc. Jpn. **52**, 4385 (1983).
[12] G. A. Saum and E. B. Hensley, Phys. Rev. **113**, 1019 (1959).
[13] J.-G. Zhang, P. C. Eklund, Z. L. Hua, L. G. Salamanca-Riba, and M. Wuttig, J. Mater. Res. **7**, 411 (1992).
[14] V. S. Stepanyuk, A. Szasz, O. V. Farberovich, A. A. Grigorenko, A. V. Kozlov, and V. V. Mikhailin, Phys. Status Solidi B **155**, 215 (1989).
[15] R. Pandey, J. E. Jaffe, and A. B. Kunz, Phys. Rev. B **43**, 9228 (1991).
[16] V. S. Stepanyuk, A. A. Grigorenko, A. A. Katsnelson, O. V. Farberovich, A. Szasz, and V. V. Mikhailin, Phys. Status Solidi B **174**, 289 (1992).
[17] A. Lichanot, A. Dargelos, and C. Larrieu, Solid State Commun. **90**, N3, 189 (1994).
[18] W. Y. Ching, F. Gan, and M.-Z. Huang, Phys. Rev. B **52**, 1596 (1995).
[19] G. Kalpana, B. Palanivel, R. M. Thomas, and M. Rajagopalan, Physica B **222**, 223 (1996).
[20] S. P. Farrell, M. E. Fleet, I. E. Stekhin, A. Kravtsova, A. V. Soldatov, and X. Liu, Am. Mineral. **87**, 1321 (2002).
[21] J. J. Rehr and R. C. Albers, Rev. Mod. Phys. **72**, 621 (2000).
[22] A. L. Ankudinov, B. Ravel, J. J. Rehr, and S. Conradson, Phys. Rev. B **58**, 7565 (1998).
[23] H. Ebert, SPR-KKR package, Munich University, 2002.
[24] Peter Blaha, Karlheinz Schwarz, Georg K. H. Madsen, Dieter Kvasnicka, and Joachim Luitz, WIEN2K package, TU Wien, 2002.
[25] E. L. Shirley, Phys. Rev. Lett. **80**, 794 (1998).
[26] Y. Joly, Phys. Rev. B **63**, 125120 (2001).
[27] H. Modrow, S. Bucher, J. J. Rehr, and A. L. Ankudinov, Phys. Rev. B **67**, 035123 (2003).
[28] F. Decremps, F. Datchi, A. M. Saitta, A. Polian, S. Pascarelli, A. Di Cicco, J. P. Itie, and F. Baudelet, Phys. Rev. B **68**, 104101 (2003).
[29] B. Sonntag and F. C. Brown, Phys. Rev. B **10**, 2300 (1974).
[30] F. Hofer and P. Golob, Ultramicroscopy **21**, 379 (1987).
[31] M. Kasrai, M. E. Fleet, T. K. Sham, G. M. Bancroft, K. H. Tan, and J. R. Broun, Solid State Commun. **68**, 507 (1988).
[32] S. P. Farrell and M. E. Fleet, Solid State Commun. **113**, 69 (2000).
[33] G. M. Bancroft, Can. Chemi. News **44**, 15 (1992).
[34] B. X. Yang, F. H. Middleton, B. G. Olsson, G. M. Bancroft, J. M. Chen, T. K. Sham, K. Tan, and D. J. Wallace, Nucl. Instrum. Methods Phys. Res. A **316**, 422 (1992).
[35] K. H. Tan, G. M. Bancroft, L. L. Coatsworth, and B. W. Yates, Can. J. Phys. **60**, 131 (1982).
[36] J. Kawai, H. Adachi, S. Hayakawa, S. Y. Zhen, K. Kobayashi, Y. Gohshi, K. Maeda, and Y. Kitajima, Spectrochim. Acta, Part B **49**, 739 (1994).
[37] M. Kasrai, R. W. Brunner, G. M. Bancroft, W. N. Lennard, J. A. Bardwell, and K. H. Tan, Appl. Surf. Sci. **99**, 303 (1996).
[38] T. Tyliszcak, BAN Data Analysis Program, McMaster University (1992).
[39] *Unoccupied Electronic States: Fundamentals for XANES, EELS, IPS and BIS*, edited by J. C. Fuggle and J. E. Inglesfield, Vol. 69 of *Topics in Applied Physics* (Springer, New York, 1992), p. 360.
[40] *CRC Handbook of Chemistry and Physics*, 67th ed., edited by R. C. Weast (CRC Press, Boca Raton, 1986), p. F116.
[41] Hitoshi Ita, Toshio Akai, Hideo Namita, Shoji Yamaguchi, and Masahary Nomura, J. Power Sources **119–121**, 567 (2003).
[42] M. Bonnin-Mosbah, N. Metrich, J. Susini, M. Salome, D. Massare, and B. Menez, Spectrochim. Acta, Part B **57**, 711 (2002).
[43] S. Della Longa, A. V. Soldatov, M. Pompa, and A. Bianconi, Comput. Mater. Sci. **4**, 199 (1995).
[44] F. Mattheiss, Phys. Rev. **181**, 987 (1969).

[45] W. Drube, T. K. Sham, A. Kravtsova, and A. V. Soldatov, Phys. Rev. B **67**, 035122 (2003).
[46] A. N. Mansour, A. Marcelli, G. Cibin, G. Yalovega, T. Sevastyanova, and A. V. Soldatov, Phys. Rev. B **65**, 134207 (2002).
[47] M. Riedler, A. R. B. de Castro, A. Kolmakov, J. O. Löfken, C. Nowak, A. V. Soldatov, A. Wark, G. Yalovega, and T. Möller, Phys. Rev. B **64**, 245419 (2001).
[48] J. E. Muller, O. Jepsen, and J. W. Wilkins, Solid State Commun. **42**, 365 (1982).
[49] J. Fink, Th. Muller-Heinzerling, B. Scheerer, W. Speier, F. U. Hillebrecht, J. C. Fuggle, J. Zaanen, and G. A. Sawatzky, Phys. Rev. B **32**, 4899 (1985).
[50] J. Schitalla and H. Ebert, Phys. Rev. Lett. **80**, 4586 (1998).
[51] A. L. Ankudinov, A. I. Nesvizhskii, and J. J. Rehr, Phys. Rev. B **67**, 115120 (2003).
[52] P. J. Durham, in *X-ray Absorption: Principles, Applications and Techniques of EXAFS, SEXAFS and XANES*, edited by R. Prins and D. C. Koningsberger (Wiley, New York, 1988).
[53] Miguel Castro, Shu-Rong Liu, Hua-Jin Zhai, and Lai-Sheng Wang, J. Chem. Phys. **188**, 2116 (2003).
[54] A. N. Kravtsova, I. E. Stekhin, A. V. Soldatov, X. Liu, and M. E. Fleet, Phys. Status Solidi B **234**, R4 (2002).
[55] Weidong Luo, Sohrab Ismail-Beigi, Marvin L. Cohen, and Steven G. Louie, Phys. Rev. B **66**, 195215 (2002).
[56] G. Schutz, W. Wagner, W. Wilhelm, P. Kienle, R. Zeller, R. Frahm, and G. Materlik, Phys. Rev. Lett. **58**, 737 (1987).
[57] K. Hamalainen, C.-C. Kao, J. B. Hastings, D. P. Siddons, L. E. Berman, V. Stojanoff, and S. P. Cramer, Phys. Rev. B **46**, 14 274 (1992).
[58] A. V. Soldatov, T. S. Ivanchenko, A. P. Kovtun, S. Della Longa, and A. Bianconi, Phys. Rev. B **52**, 11 757 (1995).
[59] A. V. Soldatov and A. N. Gusatinskii, Phys. Status Solidi B **125**, k129 (1984).
[60] A. V. Soldatov, T. S. Ivanchenko, S. Della Longa, A. Kotani, Y. Iwamoto, and A. Bianconi, Phys. Rev. B **50**, 5074 (1994).
[61] N. A. Povahznaja, I. G. Shvejtzer, and A. V. Soldatov, J. Phys.: Condens. Matter **7**, 53 (1995).
[62] A. V. Soldatov, M. Kasrai, and G. M. Bancroft, Solid State Commun. **115**, 687 (2000).